JACS
JOURNAL OF THE AMERICAN CHEMICAL SOCIETY
pubs.acs.org/JACS

Article

Mechanical and Covalent Tailoring of Copper Catenanes for Selective Aqueous Nitrate-to-Ammonia Electrocatalysis

Yulin Deng,‖ Xiaoyong Mo,‖ Samuel Kin-Man Lai, Shu-Chih Haw, Ho Yu Au-Yeung,* and Edmund C. M. Tse*

Cite This: J. Am. Chem. Soc. 2025, 147, 14316−14325

Read Online

ACCESS | Metrics & More | Article Recommendations | Supporting Information

ABSTRACT: Electrocatalytic nitrate reduction reaction (NO_3RR) for the selective generation of ammonia (NH_3) enables the removal of deleterious nitrate pollutants while simultaneously upcycling them into a value-added fertilizer. The development of nonprecious metal-derived catalysts such as those featuring copper (Cu) as earth-abundant alternatives for the state-of-the-art precious metal catalysts is of urgent need yet suffering from the activity−selectivity−durability trilemma. Rational design of molecular Cu complexes with well-defined coordination structures permitting systematic structure−activity relationship (SAR) investigations is key to addressing the challenge. Here, a series of molecular Cu(I) complexes with [2]catenane ligands are developed as NO_3RR electrocatalysts for the first time. By engineering multiple cationic ammoniums on the catenane backbone, acceptance of the anionic nitrate substrate as well as the release of the cationic ammonium product are promoted, thereby facilitating a higher Faradaic efficiency and product selectivity toward ammonia via an $8e^-$ pathway. Of note, the mutual Coulombic repulsion between the multiply charged ligands is overcome by the mechanical interlocking such that the catalyst integrity can be maintained under practical conditions. This report highlights the promise of employing mechanically interlocked ligands as a platform for customizing metal complexes as catalysts for redox processes involving multiple proton-coupled electron transfer steps.

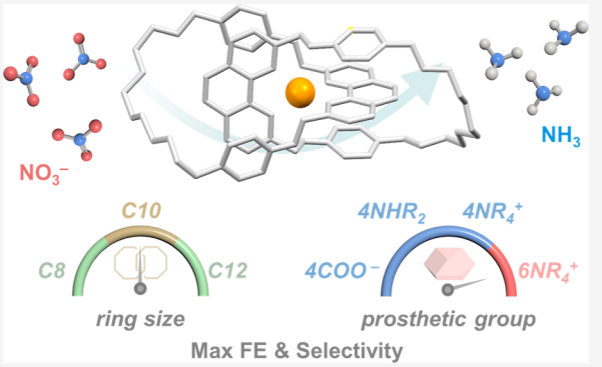

INTRODUCTION

Closing the artificial nitrogen cycle is the key to a sustainable society. The efficient removal of excessive nitrate (NO_3^-) and other nitrogen-containing pollutants from effluents, as well as their simultaneous upcycling into a value-added fertilizer (e.g., ammonia, NH_3), is one central technology for achieving this goal.[1−3] The efficient and selective electrocatalytic nitrate-to-ammonia conversion offers the opportunity for further generation of value-added nitrogen-containing organic compounds (NOCs) by harnessing ammonia from nitrate waste, including the production of ammonium carboxylates via reaction with carboxylic acids, the synthesis of urea in the presence of CO_2 or carbonates, and metal-catalyzed amination in organic synthesis. In contrast to some common strategies for nitrate removal such as membrane technology, reverse osmosis, electrodialysis, and biological denitrification,[4−10] electrocatalytic nitrate reduction is an environmentally friendly alternative that can remove and convert nitrate into ammonia via consecutive proton-coupled electron transfer (PCET) ($NO_3^- + 9H^+ + 8e^- \rightarrow NH_3 + 3H_2$) under ambient conditions without additional oxygenation processes.[11−15] Although the low-temperature nitrate-to-ammonia conversion method is promising, developing catalysts with high activity and selectivity toward ammonia remains challenging due to (1) the sluggish reduction kinetics, (2) multiple parallel pathways generating a mixture of products, and (3) the competing hydrogen evolution reaction (HER) at the cathode.[16−20]

Currently, clusters, nanoalloys, and nanoparticles derived from precious metals such as Pt, Pd, Ru, and Rh remain the major class of efficient and selective electrocatalysts for the nitrate reduction reaction (NO_3RR), in which Faradaic efficiency (FE) can reach as high as 100%.[21−24] Yet, the high cost of these precious metals has prohibited their practical application, and nonprecious metal (NPM) catalysts as cost-effective and scalable alternatives for NO_3RR have attracted immense research interest.[25] Copper (Cu) is particularly attractive due to its low cost, earth abundance, strong nitrate adsorption capability, and fast electron transfer kinetics. While Cu-based catalysts such as nanoalloys are promising for NO_3RR,[26−33] the activity−selectivity−durability trilemma remains hard to overcome due to the limitations in the

Received: December 26, 2024
Revised: April 10, 2025
Accepted: April 10, 2025
Published: April 22, 2025

https://doi.org/10.1021/jacs.4c18547
J. Am. Chem. Soc. 2025, 147, 14316−14325

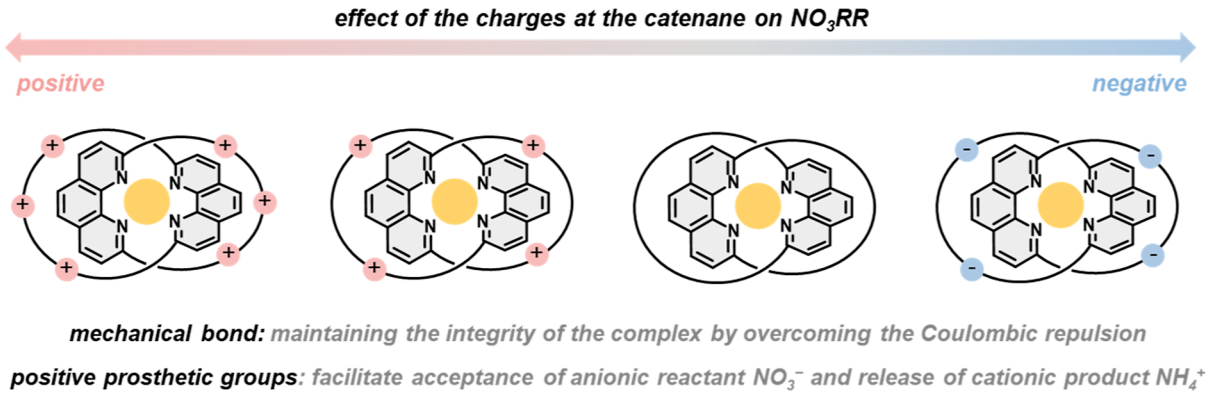

Figure 1. Effect of prosthetic groups of the Cu(I) catenane complexes on electrocatalytic nitrate reduction.

precise, atomic-level tuning of the active site structure in these catalysts composed of bulk and nanoscale copper.[34,35]

In contrast, molecular transition metal complexes are amenable for structure–activity relationship (SAR) investigations via systematic, rational ligand design to allow for more precise control and tuning of the catalytic performance. Inspired by the active site structure of copper nitrite reductases, for example, Cu(II)-bis(pyridyl)amine complexes have been utilized for the selective reduction of nitrite (NO_2^-) into NO, and the relationship between the primary coordination structure and catalytic performance has been revealed by SAR studies using various ligand analogues.[36] Copper(II) phthalocyanines have also been shown to enable NO_3RR.[37−39] Yet, different from the deeply buried metal active sites in metalloenzymes,[40−43] molecular copper complexes are usually labile, and the rapid ligand exchange involving Cu^+ or Cu^{2+} ions could often generate coordinatively ill-defined copper species during the catalysis,[44,45] which not only complicate the SAR and mechanistic understanding of the NO_3RR, but also the activity, selectivity, and durability of the catalyst are compromised.

Contrary to covalent modifications, mechanical interlocking is a conceptually different but effective way to circumvent issues related to labile copper exchange.[46−49] Due to the interlocking, ligand dissociation and exchange are sufficiently inhibited, and the coordinated metal is kinetically stabilized.[50−55] A well-defined coordination environment is thus maintained for sustaining the catalyst lifetime, minimizing side-reactivity, and extending the catalyst durability, despite there being a continuous change in the oxidation state, coordination number, and geometry of the copper during the catalysis.[55,56] On the other hand, the dynamic coordination could also control substrate access, orient substrate in a specific direction, promote product elimination, and facilitate H^+/e^- transfer for faster turnover, thereby enhancing the overall activity and selectivity.[57,58]

Herein, we report a study of enhancing the activity and selectivity of molecular Cu(I) catalysts for electrocatalytic NO_3RR via the incorporation of electrically charged prosthetic groups on catenane ligands. While dissociation of the positively charged, mutually repelling ligands is prohibited by the mechanical interlocking and structural integrity of the molecular catalysts is maintained, acceptance of the negatively charged substrate (NO_3^-), as well as release of the positively charged product (NH_4^+), is also facilitated, resulting in promoted catalytic activity and product selectivity (Figure 1).[59] In addition, the size of the interlocked macrocycles in the entangled ligands is also shown to influence the catalytic activity and selectivity of the Cu(I) catenanes.[56,57,60]

RESULTS AND DISCUSSION

Catalyst Design and Synthesis. A series of Cu(I) catenane complexes, differing by the number of cationic ammonium groups as well as the size of the interlocked macrocycles, were synthesized and studied as electrocatalysts for NO_3RR (Figures 2 and 6a). Of note, due to the mutual

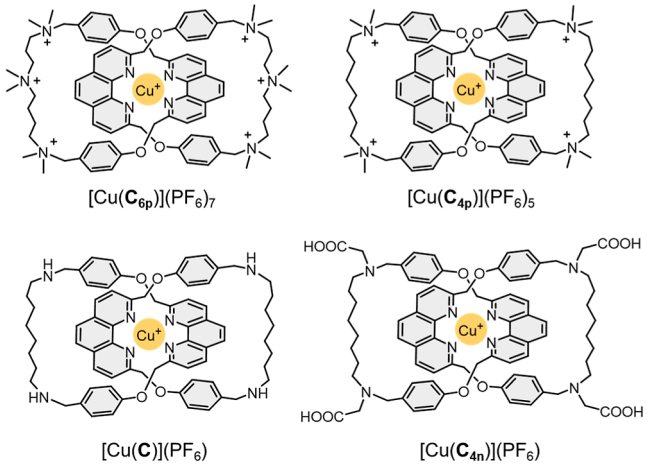

Figure 2. Structures of the Cu(I) catenane electrocatalysts. [Cu-($\mathbf{C_{6p}}$)]$(PF_6)_7$ and [Cu($\mathbf{C_{4p}}$)]$(PF_6)_5$ are supported by a [2]catenane ligand that incorporates six and four ammonium units, respectively. [Cu($\mathbf{C_{4n}}$)](PF_6) contains four carboxylic acids that exchange with carboxylates under experimental conditions.

Coulombic repulsion between the cationic ammoniums, the structural integrity of the labile Cu(I) bis(phenanthroline) coordination is maintained only in the presence of the mechanical bond; otherwise, a dynamic mixture of Cu(I) species of various ligand stoichiometry, nuclearity, and number of coordinated solvents will result.[60] Synthesis of these Cu(I) catenane complexes is detailed in the Supporting Information.[61]

Effects of the cationic ammonium groups on the structures of the complexes are studied by ^1H NMR (Figure 3). Due to the electrostatic repulsion between the ammoniums in [Cu($\mathbf{C_{6p}}$)]$(PF_6)_7$ and [Cu($\mathbf{C_{4p}}$)]$(PF_6)_5$, the interlocked macrocycles in these complexes are likely adopting a more "open" conformation when compared to [Cu($\mathbf{C}$)](PF_6). More downfield resonances (by 0.28−0.37 ppm) were found for the

https://doi.org/10.1021/jacs.4c18547
J. Am. Chem. Soc. 2025, 147, 14316−14325

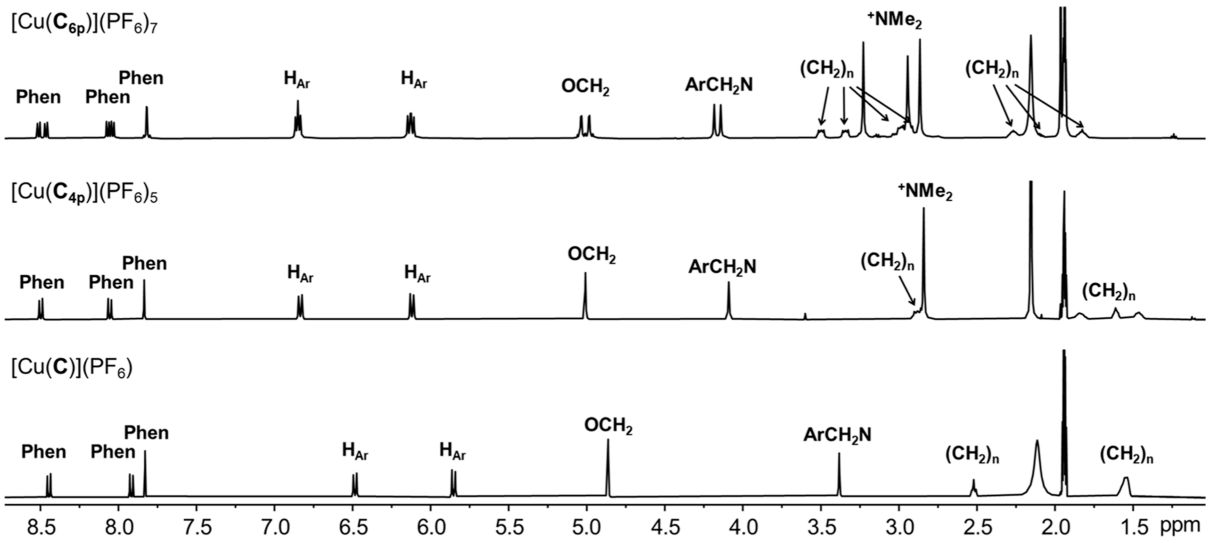

Figure 3. ^{1}H NMR spectra (500 MHz, CD_3CN, 298 K) of $[Cu(\mathbf{C_{6p}})](PF_6)_7$, $[Cu(\mathbf{C_{4p}})](PF_6)_5$, and $[Cu(\mathbf{C})](PF_6)$.

H_{Ar} protons in $[Cu(\mathbf{C_{6p}})](PF_6)_7$ and $[Cu(\mathbf{C_{4p}})](PF_6)_5$, which is consistent with a looser stacking between the phenyl and phenanthroline units. Of note, the sample of $[Cu(\mathbf{C_{6p}})](PF_6)_7$ is a racemic mixture of opposite mechanical chirality due to the directionality in the macrocycles, which is evidenced by the diastereotopic splitting of the OCH_2 and $ArCH_2N$ resonances.

Effects of the cationic ammonium groups on the redox properties of the Cu(I) catenane complexes are explored by X-ray techniques and voltammetry. X-ray photoelectron spectra (XPS) of $[Cu(\mathbf{C_{6p}})](PF_6)_7$, $[Cu(\mathbf{C_{4p}})](PF_6)_5$, $[Cu(\mathbf{C})](PF_6)$, and $[Cu(\mathbf{C_{4n}})](PF_6)$ showed that Cu is in the 1+ oxidation state (BE = ca. 932 eV) in all these catenanes (Figures 4 and S17). Cu L3-edge X-ray absorption spectroscopy (XAS) conducted in total electron yield (TEY) mode on pristine $[Cu(\mathbf{C_{6p}})](PF_6)_7$ and its carbon-supported version ($[Cu(\mathbf{C_{6p}})](PF_6)_7$/Vulcan) also corroborated a Cu(I) center in pristine $[Cu(\mathbf{C_{6p}})](PF_6)_7$ and $[Cu(\mathbf{C_{6p}})](PF_6)_7$/Vulcan, indicating that the oxidation state of the Cu(I) in the catenanes is not affected upon physical adsorption on mesoporous Vulcan. The electrochemical behavior of $[Cu(\mathbf{C_{4n}})](PF_6)$, $[Cu(\mathbf{C})](PF_6)$, and $[Cu(\mathbf{C_{6p}})](PF_6)_7$ is further investigated using cyclic voltammetry (CV) in N_2-saturated, 5× phosphate-buffered saline (PBS) buffer at pH 7. Estimated pK_a values of the four carboxyl groups in $[Cu(\mathbf{C_{4n}})](PF_6)$ are 1.6, 2.8, 4.4, and 6.1, suggesting that ca. 90% of the catenane complexes are fully deprotonated with four COO^- pendants under the CV condition. The CV curves of $[Cu(\mathbf{C_{6p}})](PF_6)_7$/Vulcan, $[Cu(\mathbf{C})](PF_6)$/Vulcan, and $[Cu(\mathbf{C_{4n}})](PF_6)$/Vulcan showed cathodic peak potentials (E_{pc}) at 0.62, 0.58, and 0.58 V vs reversible hydrogen electrode (RHE), respectively. The more positive E_{pc} of $[Cu(\mathbf{C_{6p}})](PF_6)_7$ suggests that the Cu(II/I) reduction is thermodynamically more favorable with the cationic catenane.[60] A similar positive shift is also observed when the CV was conducted using unsupported complexes in MeCN (Figure S18).

Effect of Ammonium Groups on the Electrocatalytic Nitrate Reduction Activity and Product Selectivity of Mechanically Interlocked Cu Complexes. The electrocatalytic nitrate reduction performance and effects of the charged prosthetic groups were evaluated by using $[Cu(\mathbf{C_{4p}})](PF_6)_5$/Vulcan, $[Cu(\mathbf{C})](PF_6)$/Vulcan, and $[Cu(\mathbf{C_{4n}})](PF_6)$/Vulcan as the catalysts by linear sweep voltammetry (LSV).

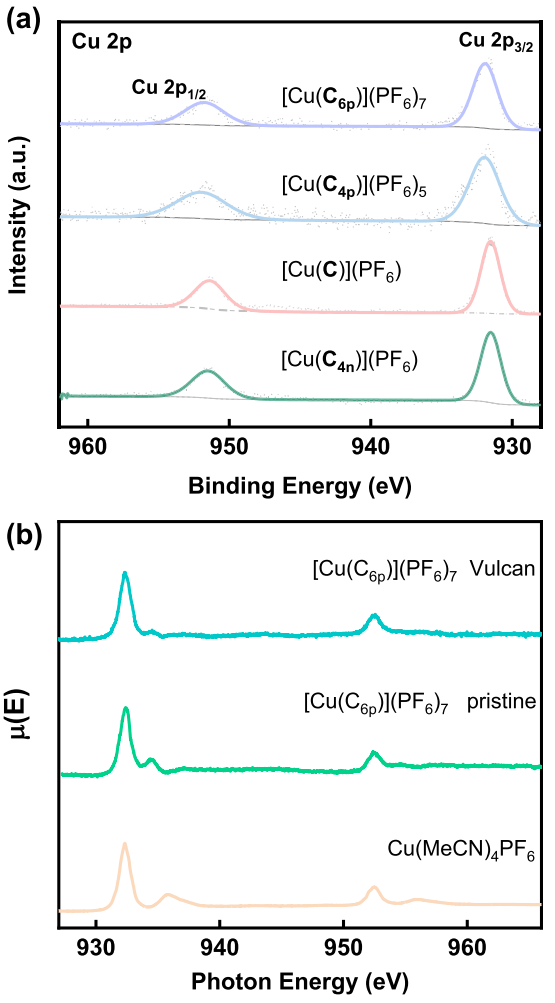

Figure 4. (a) High-resolution X-ray photoelectron spectra (XPS) of Cu 2p in $[Cu(\mathbf{C_{6p}})](PF_6)_7$ (purple), $[Cu(\mathbf{C_{4p}})](PF_6)_5$ (blue), $[Cu(\mathbf{C})](PF_6)$ (pink), and $[Cu(\mathbf{C_{4n}})](PF_6)$ (green). (b) Cu L3-edge XAS of $Cu(MeCN)_4(PF_6)$ reference (orange), $[Cu(\mathbf{C_{6p}})](PF_6)_7$ pristine (green), and $[Cu(\mathbf{C_{6p}})](PF_6)_7$ supported on Vulcan (blue). XAS spectra were collected in TEY mode.

https://doi.org/10.1021/jacs.4c18547
J. Am. Chem. Soc. 2025, 147, 14316−14325

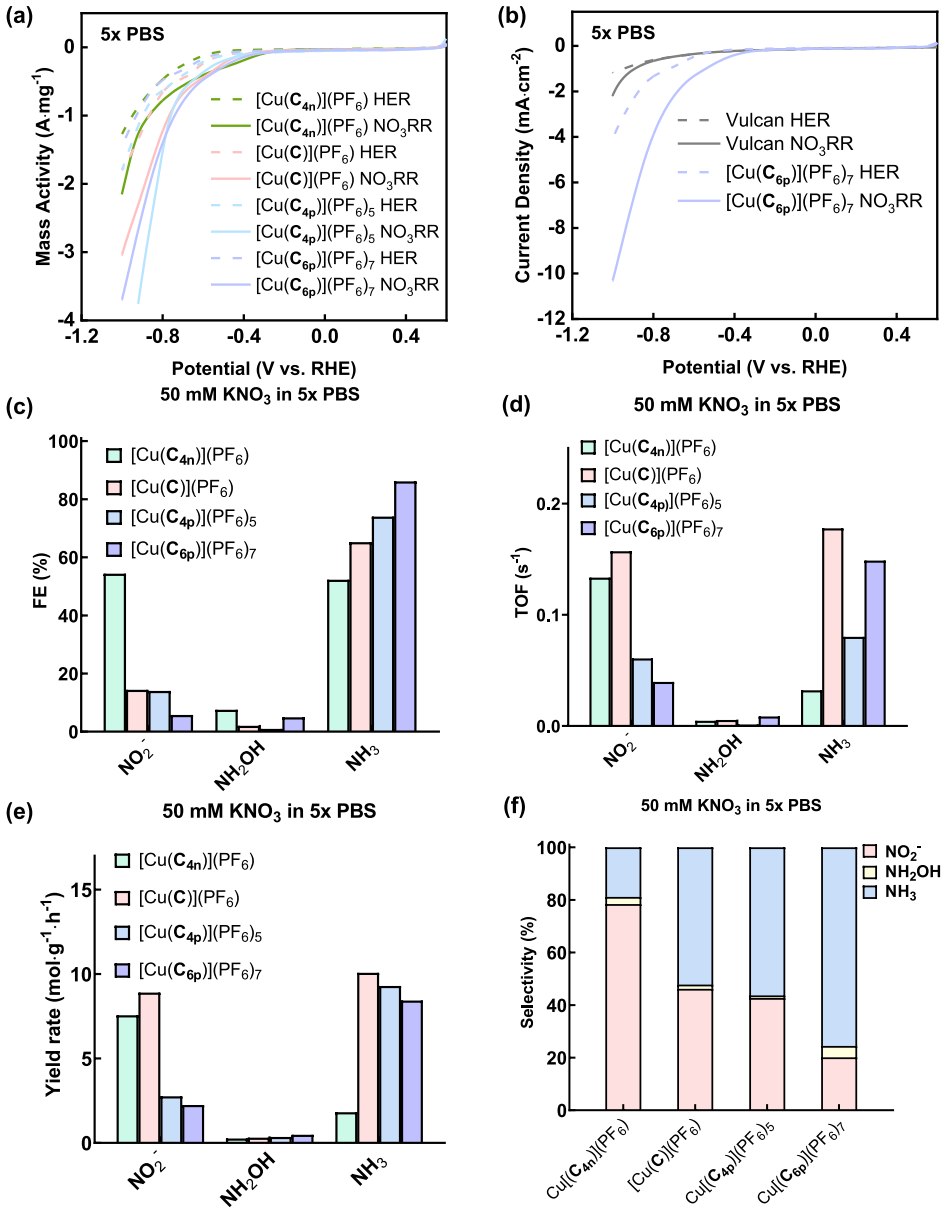

Figure 5. Impact of charged substituents on the electrocatalytic performance of the Cu(I) catenanes. (a) Mass activity of NO_3RR (solid line) and HER (dashed line) in pH 7 Ar-saturated 5× PBS catalyzed by $[Cu(\mathbf{C_{4n}})](PF_6)$ (green), $[Cu(\mathbf{C})](PF_6)$ (pink), $[Cu(\mathbf{C_{4p}})](PF_6)_5$ (blue), and $[Cu(\mathbf{C_{6p}})](PF_6)_7$ (purple). (b) Comparison of HER and NO_3RR performance of the $[Cu(\mathbf{C_{6p}})](PF_6)_7$ catalyst and Vulcan only. (c) Faradaic efficiency (FE), (d) turnover frequency (TOF), and (e) yield rate of NH_3, NH_2OH, and NO_2^- obtained by $[Cu(\mathbf{C_{4n}})](PF_6)$ (green), $[Cu(\mathbf{C})](PF_6)$ (pink), $[Cu(\mathbf{C_{4p}})](PF_6)_5$ (blue), and $[Cu(\mathbf{C_{6p}})](PF_6)_7$ (purple) at −0.8 V vs RHE. (f) Product selectivity of $[Cu(\mathbf{C_{4n}})](PF_6)$, $[Cu(\mathbf{C})](PF_6)$, $[Cu(\mathbf{C_{4p}})](PF_6)_5$, and $[Cu(\mathbf{C_{6p}})](PF_6)_7$ at −0.8 V vs RHE.

The catalytic activities are normalized on a per mass of Cu basis. In the absence of nitrate, the onset potentials of the hydrogen evolution reaction (HER) for all three Cu(I) catenane complexes are observed at −0.53 V vs RHE (Figure 5a, dashed line). Upon addition of nitrate, all as-prepared Cu(I) complexes displayed a positive shift in the onset potentials to −0.38 V vs RHE, with a concomitant increase in the mass activities, indicating that NO_3RR likely overtakes HER as the dominant and more facile process when nitrate is present. A significantly higher NO_3RR activity was found for $[Cu(\mathbf{C_{4p}})](PF_6)_5$ compared with $[Cu(\mathbf{C})](PF_6)$ and $[Cu(\mathbf{C_{4n}})](PF_6)_5$ (Figure 5). In addition, a higher NO_3^- conversion rate (by ∼7-fold) was found for $[Cu(\mathbf{C_{6p}})](PF_6)_7$/Vulcan when compared with the other Cu(I) catalysts (Figure S28a). These results suggest that the positively charged appendages on the catenanes indeed impact the electrocatalytic NO_3RR activity of the Cu(I) catalysts. Further comparing the NO_3RR of $[Cu(\mathbf{C_{6p}})](PF_6)_7$ and $[Cu(\mathbf{C_{4p}})](PF_6)_5$, a more positive onset potential (by ∼50 mV) was found in the normalized LSV of $[Cu(\mathbf{C_{6p}})](PF_6)_7$ at the same mass activity of 0.5 $A{\cdot}mg^{-1}$, corroborating that $[Cu(\mathbf{C_{6p}})](PF_6)_7$, containing the highest number of cationic ammoniums on the catenane, is the most efficient for electrocatalytic NO_3RR among all of the tested Cu(I) catenanes.

Products generated from the NO_3RR were next analyzed and compared to further understand the effects of the charged catenanes on the selectivity. After holding the Cu(I) catenane complexes at −0.8 V vs RHE for 30 min (Figure S27), the

https://doi.org/10.1021/jacs.4c18547
J. Am. Chem. Soc. 2025, 147, 14316−14325

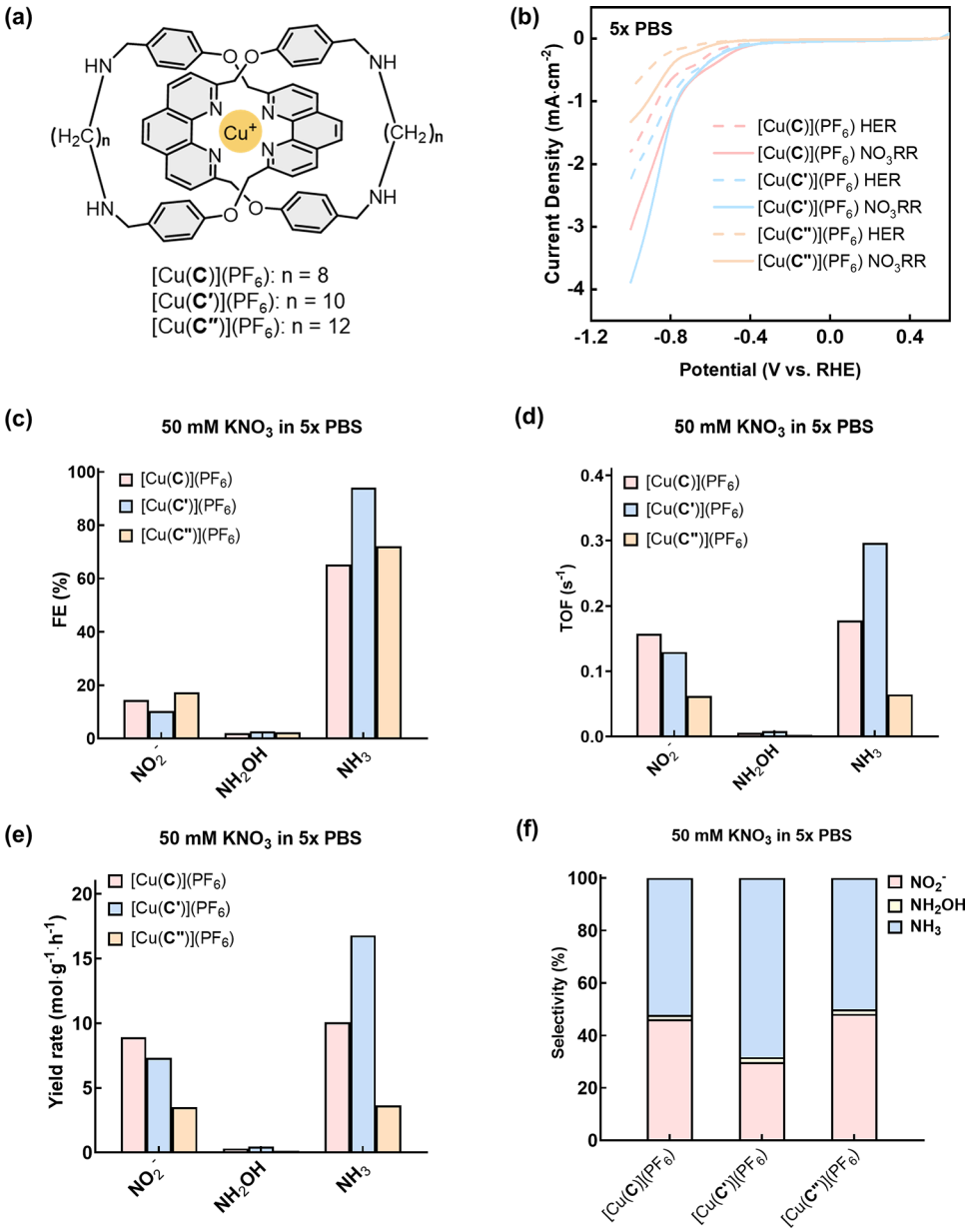

Figure 6. Impact of mechanical bond tightness on the electrocatalytic performance of Cu catenanes. (a) Structures of Cu(I) catenane complexes with different sizes of the interlocked macrocycles. (b) Mass activity with NO_3RR (solid line) and HER (dashed line) in pH 7 Ar-saturated 5× PBS catalyzed by $[Cu(\mathbf{C})](PF_6)$ (pink), $[Cu(\mathbf{C}')](PF_6)$ (blue), and $[Cu(\mathbf{C}'')](PF_6)$ (orange). (c) Faradaic efficiency (FE), (d) turnover frequency (TOF), and (e) yield rates of NH_3, NH_2OH, and NO_2^- obtained by $[Cu(\mathbf{C})](PF_6)$ (pink), $[Cu(\mathbf{C}')](PF_6)$ (blue), and $[Cu(\mathbf{C}'')](PF_6)$ (orange) at −0.8 V vs RHE. (f) Product selectivity of $[Cu(\mathbf{C})](PF_6)$, $[Cu(\mathbf{C}')](PF_6)$, and $[Cu(\mathbf{C}'')](PF_6)$ at −0.8 V vs RHE.

three main NO_3RR products, namely, nitrite (NO_2^-), hydroxylamine (NH_2OH), and ammonia (NH_3), were detected and quantified. For $[Cu(\mathbf{C_{4n}})](PF_6)$/Vulcan, similar Faradaic efficiencies (FE) for NO_2^- and NH_3 were obtained, suggesting a nonselective nitrate reduction. In contrast, $[Cu(\mathbf{C})](PF_6)$/Vulcan, $[Cu(\mathbf{C_{4p}})](PF_6)_5$/Vulcan, and $[Cu(\mathbf{C_{6p}})](PF_6)_7$/Vulcan exhibited a much higher FE for NH_3 of ca. 65%, 74%, and 86%, respectively, with a low FE for NO_2^- of ca. 14%, 14%, and 5%, respectively. As such, $[Cu(\mathbf{C_{6p}})](PF_6)_7$ displays the highest selectivity toward NH_3 (76%) when compared to $[Cu(\mathbf{C})](PF_6)$ (52%), $[Cu(\mathbf{C_{4p}})](PF_6)_5$ (56%), and $[Cu(\mathbf{C_{4n}})](PF_6)$ (19%) (Figure 5). Only a small amount of NH_2OH was detected in all of these cases. On the other hand, the turnover frequency (TOF) and yield rate of $[Cu(\mathbf{C_{6p}})](PF_6)_7$ are comparable to those of $[Cu(\mathbf{C})](PF_6)$ and much higher than those of $[Cu(\mathbf{C_{4n}})](PF_6)$, suggesting that the NO_3^- acceptance is likely assisted by the cationic ammoniums in $[Cu(\mathbf{C_{4p}})](PF_6)_5$ and $[Cu(\mathbf{C_{6p}})](PF_6)_7$ and that the electron and proton transfer during product formation is also promoted. In contrast, the anionic carboxylates in $[Cu(\mathbf{C_{4n}})](PF_6)$ may lead to an unfavorable microenvironment for NO_3^- absorption, thereby inhibiting the subsequent NO_3^- reduction steps and limiting the overall NH_3 selectivity. These results highlight the roles of charged prosthetic groups on coordination ligands in control of the activity and selectivity of transition metal catalysts beyond the primary coordination sphere. Similar strategies of exploiting electrostatic interactions in stabilizing reaction intermediates and enhancing catalytic performances of Fe-porphyrins have also been reported.[62,63]

https://doi.org/10.1021/jacs.4c18547
J. Am. Chem. Soc. 2025, 147, 14316−14325

Kinetic isotope effect (KIE) studies were conducted to gain insights into the role of protons during the NO_3RR. Upon deuteration, minimal negative shifts by only 0.02 V in the onset potentials were observed for the tested Cu(I) catenanes, suggesting a minimal equilibrium isotope effect (Figure S26). For $[Cu(\mathbf{C_{4n}})](PF_6)$, NO_2^- remained as the dominant product upon deuteration, showing that the carboxylates have no influence on the product selectivity of Cu upon switching to pD 7. In contrast, NO_2^- emerges as the major product for $[Cu(\mathbf{C})](PF_6)$/Vulcan (72%) and $[Cu(\mathbf{C_{6p}})](PF_6)_7$/Vulcan (75%) in deutero solutions (Figure S26f). A switch in the product selectivity from NQ_3 (Q = H or D) in proteo solutions to nitrite in deutero solutions indicates that a slow proton/deuteron transfer impedes HER/DER as well as the reduction steps in the NO_3RR, thereby resulting in a partial conversion of NO_3^- into NO_2^- via a $2e^-/2H^+$ pathway. Upon switching from deutero to proteo solutions, there is a larger increase in the FE of NQ_3 for $[Cu(\mathbf{C_{6p}})](PF_6)_7$/Vulcan (~40%) when compared to $[Cu(\mathbf{C})](PF_6)$/Vulcan (~15%). The more drastic increase in the NQ_3 selectivity exhibited by $[Cu(\mathbf{C_{6p}})](PF_6)_7$/Vulcan corroborates that the cationic ammoniums on the catenanes can facilitate the downstream $8e^-/9H^+$ steps to give NH_3 after the initial NO_3^- acceptance by the Cu center.

A higher cathodic current density was observed for $[Cu(\mathbf{C_{4n}})](PF_6)$/Vulcan than for $[Cu(\mathbf{C})](PF_6)$/Vulcan and $[Cu(\mathbf{C_{6p}})](PF_6)_7$/Vulcan at −0.8 V vs RHE in deutero solutions. This trend is opposite to that observed in the proteo cases and can be rationalized also by the selectivity change. Since $[Cu(\mathbf{C_{4n}})](PF_6)$/Vulcan prefers the $2e^-/2H^+$ pathway to generate NO_2^- from NO_3^- in both pH 7 and pD 7, the current density therefore remains similar in both cases. For $[Cu(\mathbf{C})](PF_6)$/Vulcan and $[Cu(\mathbf{C_{6p}})](PF_6)_7$/Vulcan, since proton transfer is faster than deuteron transfer, there is a switch in the product selectivity from NO_2^- (via $2e^-/2H^+$ transfer) to NQ_3 (via $8e^-/9H^+$ transfer) upon changing from pD 7 to pH 7, and a corresponding increase in the cathodic currents was therefore observed. Moreover, the FE, TOF, and yield rate of NQ_3 of $[Cu(\mathbf{C})](PF_6)$/Vulcan and $[Cu(\mathbf{C_{6p}})](PF_6)_7$/Vulcan decreased, while those of nitrite increased in deutero solutions as compared with proteo solutions (Figure S26c–e). Taken together, these observations suggest that the charged appendages in $[Cu(\mathbf{C_{6p}})](PF_6)_7$ and $[Cu(\mathbf{C_{4n}})](PF_6)$ influence the Cu(I) active site regarding the NO_3^- binding and proton delivery, thereby modulating the NO_3RR activity and product selectivity.

In addition, the stability and durability of $[Cu(\mathbf{C_{6p}})](PF_6)_7$ (1 mM in MeCN, 100 mM $(^nBu_4N)(PF_6)$) were evaluated by chronoamperometry experiments (Figure S23). During the course of an 8 h chronoamperometry at −1.2 V vs NHE, a steady current density was observed. Characterizations of $[Cu(\mathbf{C_{6p}})](PF_6)_7$ by CV, UV–vis spectroscopy, ESI–MS, and ^1H NMR analysis before and after the chronoamperometry experiment indicated that the Cu(I) complex did not decompose and retained its interlocked structure under the operational potential.

Effect of the Catenane Ring Size on Electrocatalytic Nitrate Reduction Activity and Product Selectivity. Because $[Cu(\mathbf{C})](PF_6)$/Vulcan exhibited a high TOF and yield rate for nitrate-to-ammonia reduction, Cu(I) catenanes analogous to $[Cu(\mathbf{C})](PF_6)$ were further explored to study the relationship between ligand interlocking and the NO_3RR performance. In particular, kinetics and thermodynamics of the tetrahedral-to-planar geometry change involving Cu(I)-to-Cu(II) transition during PCET are likely to be influenced by the ability of the catenane to undergo co-conformational changes. The NO_3RR performance can therefore be controlled by varying the length of the flexible aliphatic linkers that affect the co-conformational flexibility of the Cu(I) catenanes. Specifically, Vulcan-supported $[Cu(\mathbf{C})](PF_6)$, $[Cu(\mathbf{C'})](PF_6)$, and $[Cu(\mathbf{C''})](PF_6)$, featuring, respectively, C_8, C_{10}, and C_{12} linkers in the catenane backbone, were investigated as electrocatalysts for NO_3RR, and their FE, TOF, yield rate, and product selectivity are shown in Figure 6. Although there is a similar onset potential (−0.38 V vs RHE) for $[Cu(\mathbf{C})](PF_6)$ and $[Cu(\mathbf{C'})](PF_6)$, the cathodic current density of $[Cu(\mathbf{C'})](PF_6)$ is higher than that of $[Cu(\mathbf{C})](PF_6)$. On the other hand, $[Cu(\mathbf{C''})](PF_6)$ is found to be less active in the NO_3RR with an additional 200 mV overpotential when compared with $[Cu(\mathbf{C})](PF_6)$ and $[Cu(\mathbf{C'})](PF_6)$. While NH_3 remains as the major product for all three Cu(I) catenane catalysts, $[Cu(\mathbf{C'})](PF_6)$ exhibited the highest FE (95%), TOF (0.30 s^{-1}), yield rate (17 mol g^{-1} h^{-1}), and hence the best NH_3 selectivity (70%). The NO_3^- conversion rate of $[Cu(\mathbf{C'})](PF_6)$ is also the highest among the three Cu(I) catenanes (Figure S28b). The trend in the NO_3RR activity and product selectivity could be rationalized by the energetics of the [2]catenanes in undergoing (co)conformational changes upon accepting NO_3^-, as well as mediating downstream reduction and intermediate conversion, and a similar dependence of the activity and selectivity on the catenane ring size is also observed previously.[56,57,60]

CONCLUSIONS

A series of molecular Cu(I) complexes supported by catenane ligands tailored for efficient electrocatalytic NO_3RR has been developed. By mechanical interlocking, cationic ammoniums were successfully introduced to the catenane skeleton to enhance the activity and selectivity of ammonia formation while maintaining the structural integrity of the catalysts. Electrochemical studies showed that $[Cu(\mathbf{C_{6p}})](PF_6)_7$, featuring a hexacationic catenane ligand, can selectively generate ammonia with a Faradaic efficiency reaching 86%, while the anionic control [i.e., $[Cu(\mathbf{C_{4n}})](PF_6)$] exhibited suppressed activity and selectivity, highlighting the benefits of introducing the positively charged groups in the NO_3RR. In addition, the NO_3RR performance of the Cu(I) catenanes was also found to be dependent on the size of the interlocked macrocycles. Taken together, these results demonstrated that the NO_3RR performance of the Cu catalysts can be enhanced via both covalent modification (chemical) and mechanical interlocking (physical) of the supporting ligands, providing new directions of catalyst design for further improvement of the NO_3RR performance. These results are valuable not only because of the rational design of Cu(I) complexes for efficient electrocatalytic reactions involving intricate proton-coupled electron transfer steps but also because of the potential of mechanically interlocked ligands as a platform for transition metal catalyst customization with molecular features that are not easily achievable by noninterlocked analogues and conventional catalyst designs.[56,57,60]

METHODS

General Methods. Chemicals for molecular synthesis were obtained from commercial sources and used as received unless otherwise stated. Sodium hydroxide (NaOH, analytical grade, Merck Millipore), Nafion perfluorinated resin solution (5 wt % in lower

https://doi.org/10.1021/jacs.4c18547
J. Am. Chem. Soc. 2025, 147, 14316–14325

aliphatic alcohols and water, containing 15−20% water, Sigma-Aldrich), sodium nitrite ($NaNO_2$, Acros Organics), ammonium chloride (NH_4Cl, A.R. Dieckmann), phenol (C_6H_5OH, Sigma-Aldrich), sodium citrate anhydrous ($Na_3C_6H_5O_7$, J&K Scientific), sodium hypochlorite solution (NaClO solution, 11−14% available chlorine, Alfa Aesar), and sodium nitroprusside [$Na_2Fe(CN)_5NO\cdot 2H_2O$, A.R. Beijing Huagongchang]. Electrochemical studies at pH 7 were performed in PBS buffer containing sodium chloride (NaCl, Dieckmann), potassium chloride (KCl, J&K Scientific), sodium hydrogen phosphate (Na_2HPO_4, Dieckmann), and potassium dihydrogen phosphate (KH_2PO_4, Dieckmann). NO_3RR experiments were conducted in the above PBS buffer with 50 mM potassium nitrate (KNO_3, Acros Organics). All buffer solutions were prepared using Milli-Q water (>18 MΩ cm) and were sparged with Ar (99.995% high purity grade, Linde HKO) for 30 min before each experiment following published methods.[34,57,64]

General Inks Preparation Method. Vulcan XC-72 carbon black (Cabot) was pretreated and soaked in 0.1 M HCl (Duksan, 37% GR) for 24 h. The acid-treated carbon black was filtered and washed using Milli-Q ultrapure water and then dried in a vacuum oven at 80 °C overnight. [Cu($\mathbf{C_{4n}}$)](PF_6), [Cu($\mathbf{C_{4p}}$)](PF_6)$_5$, [Cu($\mathbf{C_{6p}}$)](PF_6)$_7$, [Cu($\mathbf{C}$)](PF_6), [Cu($\mathbf{C'}$)](PF_6), and [Cu($\mathbf{C''}$)](PF_6) were fully dissolved in acetonitrile (RCI Labscan, AR) and mixed with the pretreated Vulcan XC-72 to form their respective carbon mixtures (30% w/w). The mixtures were sonicated for 5 min. After sonication, the mixtures were dried under vacuum at 37 °C overnight. Finely ground [Cu($\mathbf{C_{4n}}$)](PF_6), [Cu($\mathbf{C_{4p}}$)](PF_6)$_5$, [Cu($\mathbf{C_{6p}}$)](PF_6)$_7$, [Cu($\mathbf{C}$)](PF_6), [Cu($\mathbf{C'}$)](PF_6), and [Cu($\mathbf{C''}$)](PF_6) catalysts on Vulcan XC-72 (4 mg) were suspended and sonicated in 1 mL of ethanol (Scharlab, Abs) for 15 min, respectively. Nafion perfluorinated resin solution (4 μL, 5 wt % in lower aliphatic alcohols with 15−20% water, Sigma-Aldrich) was added into the well-dispersed catalyst/Vulcan in ethanol. The resulting mixture was then continuously sonicated for 10 min to form inks. Eight μL of the ink was drop-casted onto a glassy carbon electrode (A = 0.07065 cm^2, Gaoss Union), which was polished with a 3−0.5 μm alumina suspension polishing kit (Allied Tech) and further dried under a stream of N_2.[57,65,66]

Electrochemical Activity Measurements. Electrochemical studies were carried out using a CH Instruments 760E electrochemical workstation at room temperature following the published procedures. Experiments were performed in a three-compartment cell with an aqueous Ag/AgCl (3 M KCl, CHI) reference electrode separated from the working electrode by a Luggin capillary as described previously.[67] Electrochemical potentials were reported relative to the RHE by using a published protocol. A Pt-wire counter electrode was separated from the working electrode with a glass frit. Chronoamperometric measurements were conducted at −0.8 V vs RHE in 5× PBS (685 mM NaCl, 13.5 mM KCl, 50 mM Na_2HPO_4 and 9 mM KH_2PO_4) buffer solution containing 50 mM KNO_3 for 0.5 h. The volume of the electrolyte in each chamber was 4 mL. Before electrochemical tests, the electrolyte solution was sparged with Ar for 30 min to remove dissolved O_2. LSV was conducted at a scan rate of 10 mV s^{-1}. Electrolysis was performed at a given potential for a designated time period.[34]

Material Characterization. XPS was conducted using a Thermo Scientific ESCALAB QXi$^+$ XPS microprobe, and the spectra were calibrated with a binding energy of 284.8 eV for C 1s. The data were analyzed following a published protocol.[65,67] Ex-situ Cu L3-edge X-ray absorption spectroscopy (XAS) measurements were conducted in TEY mode at the TLS beamline 20A end station at the National Synchrotron Radiation Research Center (NSRRC).[68]

Product Analysis. Nitrate and nitrite concentrations were quantified by using an ion chromatograph (IC) system (Thermo Scientific ICS-1100) with an electrochemical detector (ECD). 1000 ppm of NO_3^- and NO_2^- stock solutions were prepared in Milli-Q ultrapure water, diluted to known concentrations, and injected into the IC system to obtain a series of peak areas. Standard curves were prepared by correlating the NO_3^- and NO_2^- concentrations and the peak areas.[34]

All UV−visible spectra were collected using an Implen NanoPhotometer NP80 UV−vis spectrophotometer with UVette (Eppendorf) cuvettes. Ammonia was quantified by an indophenol blue method.[69] Phenol (1.058 g) was dissolved in absolute ethanol (10 mL) to prepare a fresh phenol solution, which can be used for a week. Sodium nitroprusside (0.05 g) was dissolved in Milli-Q water (10 mL) to prepare an Fe catalyst solution. 5% NaClO solution was diluted from commercially available 11−14% NaClO using Milli-Q water. The alkaline citrate solution was prepared by dissolving NaOH (2.5 g) and trisodium citrate (50 g) in a Milli-Q water (250 mL). The alkaline oxidizing solution was prepared by mixing the alkaline citrate solution and 5% NaClO solution with a V/V ratio of 4:1. Ammonia standard solutions were prepared by diluting NH_4Cl stock solution (1000 ppm) into designated concentrations. Standard solution (0.5 mL) was diluted 5-fold using Milli-Q water. Phenol solution (0.1 mL), Fe catalyst solution (0.1 mL), and alkaline oxidizing solution (0.425 mL) were sequentially added to the diluted standard solution. After it was mixed thoroughly, the final solution was placed in the dark at room temperature for 4 h. The NH_4^+ standard curve was constructed by correlating standard solution concentrations with absorbances at 630 nm.[34,38,70] The same procedure was used to quantify the amount of NH_4^+ in the electrolysis experiment.

Hydroxylamine was quantified by a revised method with $K_3Fe(CN)_6$ under strong alkaline conditions. 0.2 mL of sample or NH_2OH standard, 0.1 mL of $K_3Fe(CN)_6$ in 100 mM KCl, and 0.3 mL of 25% KOH were mixed thoroughly following the writing sequence and reacted for 7 min. A blank control was conducted by replacing the sample with electrolyte only. The NH_2OH standard curve was constructed by correlating standard solution concentrations with absorbances at 425 nm.[70]

Product Analysis Calculations. Faradaic efficiency (%)

$$\mathrm{FE} = \frac{n \times F \times C_{\mathrm{product}} \times V}{Q} \times 100\% \tag{1}$$

where C_{product} is the concentration of each product in mol L^{-1}, V is the volume of electrolyte solution (4×10^{-3} L), n is the number of electrons required to obtain a certain product, F is the Faraday constant (96,485 C mol^{-1}), and Q is the total charge (C) passed during electrolysis.

Turnover frequency (s^{-1})

$$\mathrm{TOF} = \frac{C_{\mathrm{product}} \times V}{m_{\mathrm{catalyst}} \times t} \tag{2}$$

where C_{product} is the concentration of each product in mol L^{-1}, V is the volume of electrolyte solution (4×10^{-3} L), F is the Faraday constant (96485 C mol^{-1}), m is the number of moles of catalyst, and t is the electrolysis time in s.

Yield rate (mol g^{-1} h^{-1})

$$\mathrm{yield} = \frac{C_{\mathrm{product}} \times V}{M_{\mathrm{catalyst}} \times t} \tag{3}$$

where C_{product} is the concentration of each product in mol L^{-1}, V is the volume of electrolyte solution (4×10^{-3} L), M_{catalyst} is the mass of the Cu catalyst, and t is the electrolysis time in h.

Product selectivity (%)

$$\mathrm{selectivity} = \left(\frac{\text{moles of } N_{\mathrm{product}}}{\text{total moles of product}}\right) \times 100\% \tag{4}$$

N_{product} refers to the nitrogenous product generated.

NO_3^- conversion rate (%)

$$\eta_{NO_3^-} = \frac{C_{0,NO_3^-} - C_{NO_3^-}}{C_{0,NO_3^-}} \times 100\% \tag{5}$$

Methods for KIE Studies. All proteo and deutero aqueous solutions were prepared freshly each day using Milli-Q water (>18 MΩ cm) and D_2O, respectively. For experiments in pH 7 and pD 7,

https://doi.org/10.1021/jacs.4c18547
J. Am. Chem. Soc. 2025, 147, 14316−14325

both proteo and deutero PBS solutions containing sodium chloride (NaCl, Dieckmann), potassium chloride (KCl, J&K Scientific), sodium hydrogen phosphate (Na_2HPO_4, Dieckmann), and potassium dihydrogen phosphate (KH_2PO_4, Dieckmann) were used. NO_3RR experiments were conducted in the PBS buffer described above with 50 mM potassium nitrate (KNO_3, Acros Organics). The pH and pD values of buffer solutions were measured using a Jenway 3510 Standard Digital pH Meter calibrated with three standard buffer solutions.[67,71−73] pH readings were converted to pD using eq 6, in which pH_a is the apparent reading from the pH meter

$$pD = pH_a + 0.41 \quad (6)$$

■ ASSOCIATED CONTENT

Supporting Information

The Supporting Information is available free of charge at https://pubs.acs.org/doi/10.1021/jacs.4c18547.

Experimental data, as well as the characterization data for all of the compounds prepared in the course of these studies, experimental details, synthetic procedures, NMR and MS characterization data, control experiments, KIE studies, XPS spectra, ICP−MS results, cyclic voltammograms, linear sweep voltammograms, computational methods and results, supplementary tables, additional notes, and supporting figures (PDF)

■ AUTHOR INFORMATION

Corresponding Authors

Ho Yu Au-Yeung − *HKU-CAS Joint Laboratory on New Materials & Department of Chemistry, The University of Hong Kong, Hong Kong SAR, P. R. China; State Key Laboratory of Synthetic Chemistry, The University of Hong Kong, Hong Kong SAR, P. R. China;* orcid.org/0000-0002-7216-7921; Email: hoyuay@hku.hk

Edmund C. M. Tse − *HKU-CAS Joint Laboratory on New Materials & Department of Chemistry, The University of Hong Kong, Hong Kong SAR, P. R. China;* orcid.org/0000-0002-9313-1290; Email: ecmtse@hku.hk

Authors

Yulin Deng − *HKU-CAS Joint Laboratory on New Materials & Department of Chemistry, The University of Hong Kong, Hong Kong SAR, P. R. China;* orcid.org/0000-0003-1566-3619

Xiaoyong Mo − *HKU-CAS Joint Laboratory on New Materials & Department of Chemistry, The University of Hong Kong, Hong Kong SAR, P. R. China;* orcid.org/0000-0002-8586-4056

Samuel Kin-Man Lai − *HKU-CAS Joint Laboratory on New Materials & Department of Chemistry, The University of Hong Kong, Hong Kong SAR, P. R. China;* orcid.org/0000-0002-8959-724X

Shu-Chih Haw − *National Synchrotron Radiation Research Center, Hsinchu 30076, Taiwan*

Complete contact information is available at: https://pubs.acs.org/10.1021/jacs.4c18547

Author Contributions

‖Y.D. and X.M. contributed equally.

Notes

The authors declare no competing financial interest.

■ ACKNOWLEDGMENTS

E.C.M.T. would like to express gratitude to the Innovation and Technology Commission for an ITSP Seed Project (ITC: ITS/271/22) and a TSSSU scheme (TSSSU/HKU/23/05/2) on interfacial electrocatalysis. H.Y.A.-Y. acknowledges the support from the CAS-Croucher Funding Scheme for Joint Laboratories and the Collaborative Research Fund (C7075-21G) from the Research Grants Council (RGC) of Hong Kong. X.M. thanks the support from the Shenzhen Science and Technology Innovation Commission (SZSTI: JCYJ20210324122011031). Y.D. acknowledges the Dissertation Year Fellowship from the University of Hong Kong. The authors thank Frankie Y.F. Chan at the Electron Microscope Unit (EMU) at the University of Hong Kong (HKU) for his help with materials characterization. X.M. and E.C.M.T. acknowledge the funding support from the "Laboratory for Synthetic Chemistry and Chemical Biology" under the Health@InnoHK Program launched by ITC, HKSAR, China. The authors also thank the RGC in Hong Kong for a Theme-based Research Scheme (TRS: T23-713/22-R), an Early Career Scheme (ECS: 27301120), General Research Funds (GRF: 17308323, 17308724), and a grant from the Co-funding Mechanism on Joint Laboratories with the Chinese Academy of Sciences (CAS) (JLFS/P-701/24) for enhancing the surface characterization facility at the HKU-CAS Joint Laboratory on New Materials and supporting research activities on green electrocatalysis and clean energy conversion. UGC funding administered by The University of Hong Kong is acknowledged for support of the Electrospray Ionization Quadrupole Time-of-Flight Mass Spectrometry Facilities under the support for Interdisciplinary Research in Chemical Science. S.K.-M.L. acknowledges the high-performance computing (HPC) services offered by ITS at HKU.

■ REFERENCES

(1) Rosca, V.; Duca, M.; de Groot, M. T.; Koper, M. T. M. Nitrogen Cycle Electrocatalysis. *Chem. Rev.* **2009**, *109*, 2209−2244.

(2) Chen, F.-Y.; Elgazzar, A.; Pecaut, S.; Qiu, C.; Feng, Y.; Ashokkumar, S.; Yu, Z.; Sellers, C.; Hao, S.; Zhu, P.; Wang, H. Electrochemical nitrate reduction to ammonia with cation shuttling in a solid electrolyte reactor. *Nat. Catal.* **2024**, *7*, 1032−1043.

(3) Liu, Y.; Liu, K.; Wang, P.; Jin, Z.; Li, P. Electrocatalytic upcycling of nitrogenous wastes into green ammonia: advances and perspectives on materials innovation. *Carbon Neutrality* **2023**, *2*, 14.

(4) Belhamidi, S.; El-Ghzizel, S.; Taky, M.; Elmidaoui, A. Nitrate removal of groundwater by reverse osmosis, nanofiltration and electrodialysis: performances and cost comparison. *Desalin. Water Treat.* **2022**, *262*, 338−346.

(5) Pang, Y.; Wang, J. Various electron donors for biological nitrate removal: A review. *Sci. Total Environ.* **2021**, *794*, 148699.

(6) Scholes, R. C.; Vega, M. A.; Sharp, J. O.; Sedlak, D. L. Nitrate removal from reverse osmosis concentrate in pilot-scale open-water unit process wetlands. *Environ. Sci.: Water Res. Technol.* **2021**, *7*, 650−661.

(7) Aliaskari, M.; Schäfer, A. I. Nitrate, arsenic and fluoride removal by electrodialysis from brackish groundwater. *Water Res.* **2021**, *190*, 116683.

(8) Chen, J.; Gu, M.; Zhou, Y.; Wan, D.; He, Q.; Shi, Y.; Liu, Y. Efficient nitrate and perchlorateremoval from aqueous solution via a novel electro-dialysis ion-exchange membrane bioreactor. *J. Chem. Eng.* **2022**, *430*, 132952.

(9) Ahmed, S. M.; Rind, S.; Rani, K. Systematic review: External carbon source for biological denitrification for wastewater. *Biotechnol. Bioeng.* **2023**, *120*, 642−658.

(10) Fan, Y.; Wang, X.; Butler, C.; Kankam, A.; Belgada, A.; Simon, J.; Gao, Y.; Chen, E.; Winter, L. R. Highly efficient metal-free nitrate reduction enabled by electrified membrane filtration. *Nat. Water* **2024**, *2*, 684−696.
(11) Bai, L.; Franco, F.; Timoshenko, J.; Rettenmaier, C.; Scholten, F.; Jeon, H. S.; Yoon, A.; Rüscher, M.; Herzog, A.; Haase, F. T.; Kühl, S.; Chee, S. W.; Bergmann, A.; Beatriz, R. C. Electrocatalytic Nitrate and Nitrite Reduction toward Ammonia Using Cu_2O Nanocubes: Active Species and Reaction Mechanisms. *J. Am. Chem. Soc.* **2024**, *146*, 9665−9678.
(12) Chen, D.; Yin, D.; Zhang, S.; Yip, S.; Ho, J. C. Nitrate electroreduction: recent development in mechanistic understanding and electrocatalyst design. *Mater. Today Energy* **2024**, *44*, 101610.
(13) Gao, X.; Tse, E. C. M. Unraveling the Performance Descriptors for Designing Single-Atom Catalysts on Defective MXenes for Exclusive Nitrate-To-Ammonia Electrocatalytic Upcycling. *Small* **2024**, *20*, 2306311.
(14) Ricke, N. D.; Murray, A. T.; Shepherd, J. J.; Welborn, M. G.; Fukushima, T.; Van Voorhis, T.; Surendranath, Y. Molecular-Level Insights into Oxygen Reduction Catalysis by Graphite-Conjugated Active Sites. *ACS Catal.* **2017**, *7*, 7680−7687.
(15) Elwell, C. E.; Gagnon, N. L.; Neisen, B. D.; Dhar, D.; Spaeth, A. D.; Yee, G. M.; Tolman, W. B. Copper−Oxygen Complexes Revisited: Structures, Spectroscopy, and Reactivity. *Chem. Rev.* **2017**, *117*, 2059−2107.
(16) Zhang, S.; Wu, J.; Zheng, M.; Jin, X.; Shen, Z.; Li, Z.; Wang, Y.; Wang, Q.; Wang, X.; Wei, H.; Zhang, J.; Wang, P.; Zhang, S.; Yu, L.; Dong, L.; Zhu, Q.; Zhang, H.; Lu, J. Fe/Cu diatomic catalysts for electrochemical nitrate reduction to ammonia. *Nat. Commun.* **2023**, *14*, 3634.
(17) Daiyan, R.; Tran-Phu, T.; Kumar, P.; Iputera, K.; Tong, Z.; Leverett, J.; Khan, M. H. A.; Esmailpour, A. A.; Jalili, A.; Lim, M.; Tricoli, A.; Liu, R.-S.; Lu, X.; Lovell, E.; Amal, R. Nitrate reduction to ammonium: from CuO defect engineering to waste NO_x-to-NH_3 economic feasibility. *Energy Environ. Sci.* **2021**, *14*, 3588−3598.
(18) Jia, R.; Wang, Y.; Wang, C.; Ling, Y.; Yu, Y.; Zhang, B. Boosting Selective Nitrate Electroreduction to Ammonium by Constructing Oxygen Vacancies in TiO_2. *ACS Catal.* **2020**, *10*, 3533−3540.
(19) Garcia-Segura, S.; Lanzarini-Lopes, M.; Hristovski, K.; Westerhoff, P. Electrocatalytic reduction of nitrate: Fundamentals to full-scale water treatment applications. *Appl. Catal., B* **2018**, *236*, 546−568.
(20) Fang, Z.; Jin, Z.; Tang, S.; Li, P.; Wu, P.; Yu, G. Porous Two-dimensional Iron-Cyano Nanosheets for High-rate Electrochemical Nitrate Reduction. *ACS Nano* **2022**, *16*, 1072−1081.
(21) Martínez, J.; Ortiz, A.; Ortiz, I. State-of-the-art and perspectives of the catalytic and electrocatalytic reduction of aqueous nitrates. *Appl. Catal., B* **2017**, *207*, 42−59.
(22) Han, S.; Li, H.; Li, T.; Chen, F.; Yang, R.; Yu, Y.; Zhang, B. Ultralow overpotential nitrate reduction to ammonia via a three-step relay mechanism. *Nat. Catal.* **2023**, *6*, 402−414.
(23) de Groot, M. T.; Koper, M. T. M. The influence of nitrate concentration and acidity on the electrocatalytic reduction of nitrate on platinum. *J. Electroanal. Chem.* **2004**, *562*, 81−94.
(24) Yang, J.; Sebastian, P.; Duca, M.; Hoogenboom, T.; Koper, M. T. M. pH dependence of the electroreduction of nitrate on Rh and Pt polycrystalline electrodes. *Chem. Commun.* **2014**, *50*, 2148−2151.
(25) Bullock, R. M.; Chen, J. G.; Gagliardi, L.; Chirik, P. J.; Farha, O. K.; Hendon, C. H.; Jones, C. W.; Keith, J. A.; Klosin, J.; Minteer, S. D.; et al. Using nature's blueprint to expand catalysis with Earth-abundant metals. *Science* **2020**, *369*, No. eabc3183.
(26) Hou, T.; Shan, T.; Rong, H.; Zhang, J. Nitrate Electroreduction to Ammonia Over Copper-based Catalysts. *ChemSusChem* **2025**, No. e202402331.
(27) Wei, J.; Li, Y.; Lin, H.; Lu, X.; Zhou, C.; Li, Y.-y. Copper-based electro-catalytic nitrate reduction to ammonia from water: Mechanism, preparation, and research directions. *Environ. Sci. Ecotechnology* **2024**, *20*, 100383.
(28) Zhao, X.; Jiang, Y.; Wang, M.; Huan, Y.; Cheng, Q.; He, Y.; Qian, T.; Yan, C. Comprehensive understanding of the thriving electrocatalytic nitrate/nitrite reduction to ammonia under ambient conditions. *J. Energy Chem.* **2024**, *92*, 459−483.
(29) Yu, Z.; Gu, M.; Wang, Y.; Li, H.; Chen, Y.; Wei, L. Recent Progress of Electrochemical Nitrate Reduction to Ammonia on Copper-Based Catalysts: From Nanoparticles to Single Atoms. *Adv. Energy Sustainability Res.* **2024**, *5*, 2300284.
(30) Zhang, K.; Liu, Y.; Pan, Z.; Xia, Q.; Huo, X.; Esan, O. C.; Zhang, X.; An, L. Cu-based catalysts for electrocatalytic nitrate reduction to ammonia: fundamentals and recent advances. *EES. Catal.* **2024**, *2*, 727−752.
(31) Xu, B.; Li, D.; Zhao, Q.; Feng, S.; Peng, X.; Chu, P. K. Electrochemical reduction of nitrate to ammonia using non-precious metal-based catalysts. *Coord. Chem. Rev.* **2024**, *502*, 215609.
(32) Gao, Q.; Pillai, H. S.; Huang, Y.; Liu, S.; Mu, Q.; Han, X.; Yan, Z.; Zhou, H.; He, Q.; Xin, H.; Zhu, H. Breaking adsorption-energy scaling limitations of electrocatalytic nitrate reduction on intermetallic CuPd nanocubes by machine-learned insights. *Nat. Commun.* **2022**, *13*, 2338.
(33) Haro, D. A. C.; Barrera, L.; Iriawan, H.; Herzog, A.; Tian, N.; Medford, A. J.; Shao-Horn, Y.; Alamgir, F. M.; Hatzell, M. C. Electrocatalysts for Inorganic and Organic Waste Nitrogen Conversion. *ACS Catal.* **2024**, *14*, 9752−9775.
(34) Wang, W.; Chen, J.; Tse, E. C. M. Synergy between Cu and Co in a Layered Double Hydroxide Enables Close to 100% Nitrate-to-Ammonia Selectivity. *J. Am. Chem. Soc.* **2023**, *145*, 26678−26687.
(35) Wang, K.; Mao, R.; Liu, R.; Zhang, J.; Zhao, H.; Ran, W.; Zhao, X. Intentional corrosion-induced reconstruction of defective NiFe layered double hydroxide boosts electrocatalytic nitrate reduction to ammonia. *Nat. Water* **2023**, *1*, 1068−1078.
(36) van Langevelde, P. H.; Engbers, S.; Buda, F.; Hetterscheid, D. G. H. Elucidation of the Electrocatalytic Nitrite Reduction Mechanism by Bio-Inspired Copper Complexes. *ACS Catal.* **2023**, *13*, 10094−10103.
(37) Shi, L.; Li, Y.; He, S.; Liu, Y.; Tang, X.; Ao, L.; Lv, X.; Fu, W.; Jiang, G. Efficient electrocatalytic nitrate reduction on molecular catalyst with electron-deficient single-atom $Cu^{\delta+}$ sites. *J. Chem. Eng.* **2024**, *495*, 153427.
(38) Jiang, Z.; Wang, Y.; Lin, Z.; Yuan, Y.; Zhang, X.; Tang, Y.; Wang, H.; Li, H.; Jin, C.; Liang, Y. Molecular electrocatalysts for rapid and selective reduction of nitrogenous waste to ammonia. *Energy Environ. Sci.* **2023**, *16*, 2239−2246.
(39) Chebotareva, N.; Chebotareva, N. Metallophthalocyanine catalysed electroreduction of nitrate and nitrite ions in alkaline media. *J. Appl. Electrochem.* **1997**, *27*, 975−981.
(40) Valdez, C. E.; Smith, Q. A.; Nechay, M. R.; Alexandrova, A. N. Mysteries of Metals in Metalloenzymes. *Acc. Chem. Res.* **2014**, *47*, 3110−3117.
(41) Suzuki, S.; Kataoka, K.; Yamaguchi, K.; Inoue, T.; Kai, Y. Structure−function relationships of copper-containing nitrite reductases. *Coord. Chem. Rev.* **1999**, *190*−*192*, 245−265.
(42) Van Stappen, C.; Deng, Y.; Liu, Y.; Heidari, H.; Wang, J.-X.; Zhou, Y.; Ledray, A. P.; Lu, Y. Designing Artificial Metalloenzymes by Tuning of the Environment beyond the Primary Coordination Sphere. *Chem. Rev.* **2022**, *122*, 11974−12045.
(43) Yu, Y.; Lv, X.; Li, J.; Zhou, Q.; Cui, C.; Hosseinzadeh, P.; Mukherjee, A.; Nilges, M. J.; Wang, J.; Lu, Y. Defining the Role of Tyrosine and Rational Tuning of Oxidase Activity by Genetic Incorporation of Unnatural Tyrosine Analogs. *J. Am. Chem. Soc.* **2015**, *137*, 4594−4597.
(44) Trammell, R.; Rajabimoghadam, K.; Garcia-Bosch, I. Copper-Promoted Functionalization of Organic Molecules: from Biologically Relevant Cu/O_2 Model Systems to Organometallic Transformations. *Chem. Rev.* **2019**, *119*, 2954−3031.
(45) Santini, C.; Pellei, M.; Gandin, V.; Porchia, M.; Tisato, F.; Marzano, C. Advances in Copper Complexes as Anticancer Agents. *Chem. Rev.* **2014**, *114*, 815−862.

https://doi.org/10.1021/jacs.4c18547
J. Am. Chem. Soc. 2025, 147, 14316−14325

(46) Albrecht-Gary, A. M.; Saad, Z.; Dietrich-Buchecker, C. O.; Sauvage, J. P. Interlocked macrocyclic ligands: a kinetic catenand effect in copper(I) complexes. *J. Am. Chem. Soc.* **1985**, *107*, 3205−3209.
(47) Dietrich-Buchecker, C. O.; Kern, J.-M.; Sauvage, J.-P. An air-stable d9 nickel(I) catenate: stabilisation of monovalent nickel by interlocked macrocyclic ligands. *J. Chem. Soc., Chem. Commun.* **1985**, 760−762.
(48) Dietrich-Buchecker, C.; Sauvage, J. P.; Kern, J. M. Synthesis and electrochemical studies of catenates: stabilization of low oxidation states by interlocked macrocyclic ligands. *J. Am. Chem. Soc.* **1989**, *111*, 7791−7800.
(49) Cirulli, M.; Kaur, A.; Lewis, J. E. M.; Zhang, Z.; Kitchen, J. A.; Goldup, S. M.; Roessler, M. M. Rotaxane-Based Transition Metal Complexes: Effect of the Mechanical Bond on Structure and Electronic Properties. *J. Am. Chem. Soc.* **2019**, *141*, 879−889.
(50) Albrecht-Gary, A. M.; Dietrich-Buchecker, C.; Saad, Z.; Sauvage, J. P. Topological kinetic effects: complexation of interlocked macrocyclic ligands by cationic species. *J. Am. Chem. Soc.* **1988**, *110*, 1467−1472.
(51) Sauvage, J. P. Interlacing molecular threads on transition metals: catenands, catenates, and knots. *Acc. Chem. Res.* **1990**, *23*, 319−327.
(52) Lewis, J. E. M.; Beer, P. D.; Loeb, S. J.; Goldup, S. M. Metal ions in the synthesis of interlocked molecules and materials. *Chem. Soc. Rev.* **2017**, *46*, 2577−2591.
(53) Beves, J. E.; Blight, B. A.; Campbell, C. J.; Leigh, D. A.; McBurney, R. T. Strategies and Tactics for the Metal-Directed Synthesis of Rotaxanes, Knots, Catenanes, and Higher Order Links. *Angew. Chem., Int. Ed.* **2011**, *50*, 9260−9327.
(54) Gao, W.-X.; Feng, H.-J.; Guo, B.-B.; Lu, Y.; Jin, G.-X. Coordination-Directed Construction of Molecular Links. *Chem. Rev.* **2020**, *120*, 6288−6325.
(55) Au-Yeung, H. Y.; Deng, Y. Distinctive features and challenges in catenane chemistry. *Chem. Sci.* **2022**, *13*, 3315−3334.
(56) Zhu, L.; Li, J.; Yang, J.; Au-Yeung, H. Y. Cross dehydrogenative C−O coupling catalysed by a catenane-coordinated copper(I). *Chem. Sci.* **2020**, *11*, 13008−13014.
(57) Mo, X.; Deng, Y.; Lai, S. K.-M.; Gao, X.; Yu, H.-L.; Low, K.-H.; Guo, Z.; Wu, H.-L.; Au-Yeung, H. Y.; Tse, E. C. M. Mechanical Interlocking Enhances the Electrocatalytic Oxygen Reduction Activity and Selectivity of Molecular Copper Complexes. *J. Am. Chem. Soc.* **2023**, *145*, 6087−6099.
(58) Hsueh, F.-C.; Tsai, C.-Y.; Lai, C.-C.; Liu, Y.-H.; Peng, S.-M.; Chiu, S.-H. N-Heterocyclic Carbene Copper(I) Rotaxanes Mediate Sequential Click Ligations with All Reagents Premixed. *Angew. Chem., Int. Ed.* **2020**, *59*, 11278−11282.
(59) Fan, J.; Arrazolo, L. K.; Du, J.; Xu, H.; Fang, S.; Liu, Y.; Wu, Z.; Kim, J.-H.; Wu, X. Effects of Ionic Interferents on Electrocatalytic Nitrate Reduction: Mechanistic Insight. *Environ. Sci. Technol.* **2024**, *58*, 12823−12845.
(60) Tang, M. P.; Zhu, L.; Deng, Y.; Shi, Y.-X.; Lai, S. K.-M.; Mo, X.; Pang, X.-Y.; Liu, C.; Jiang, W.; Tse, E. C. M.; Au-Yeung, H. Y. Water and Air Stable Copper(I) Complexes of Tetracationic Catenane Ligands for Oxidative C−C Cross-Coupling. *Angew. Chem., Int. Ed.* **2024**, *63*, No. e202405971.
(61) Yee, C.-C.; Ng, A. W. H.; Au-Yeung, H. Y. Control over the macrocyclisation pathway and product topology in a copper-templated catenane synthesis. *Chem. Commun.* **2019**, *55*, 6169−6172.
(62) Azcarate, I.; Costentin, C.; Robert, M.; Savéant, J.-M. Through-Space Charge Interaction Substituent Effects in Molecular Catalysis Leading to the Design of the Most Efficient Catalyst of CO_2-to-CO Electrochemical Conversion. *J. Am. Chem. Soc.* **2016**, *138*, 16639−16644.
(63) Khadhraoui, A.; Gotico, P.; Boitrel, B.; Leibl, W.; Halime, Z.; Aukauloo, A. Local ionic liquid environment at a modified iron porphyrin catalyst enhances the electrocatalytic performance of CO_2 to CO reduction in water. *Chem. Commun.* **2018**, *54*, 11630−11633.
(64) Wang, S.; Gao, X.; Mo, X.; Phillips, D. L.; Tse, E. C. M. Immobilization of a Molecular Copper Complex and a Carboxylate-Terminated Cocatalyst on a Metal Oxide Electrode for Enhanced Electrocatalytic Oxygen Reduction. *ACS Catal.* **2023**, *13*, 5599−5608.
(65) Varnell, J. A.; Tse, E. C. M.; Schulz, C. E.; Fister, T. T.; Haasch, R. T.; Timoshenko, J.; Frenkel, A. I.; Gewirth, A. A. Identification of carbon-encapsulated iron nanoparticles as active species in non-precious metal oxygen reduction catalysts. *Nat. Commun.* **2016**, *7*, 12582.
(66) Tse, E. C. M.; Schilter, D.; Gray, D. L.; Rauchfuss, T. B.; Gewirth, A. A. Multicopper Models for the Laccase Active Site: Effect of Nuclearity on Electrocatalytic Oxygen Reduction. *Inorg. Chem.* **2014**, *53*, 8505−8516.
(67) Mo, X.; Gao, X.; Gillado, A. V.; Chen, H.-Y.; Chen, Y.; Guo, Z.; Wu, H.-L.; Tse, E. C. M. Direct 3D Printing of Binder-Free Bimetallic Nanomaterials as Integrated Electrodes for Glycerol Oxidation with High Selectivity for Valuable C_3 Products. *ACS Nano* **2022**, *16*, 12202−12213.
(68) Chou, T.-C.; Chang, C.-C.; Yu, H.-L.; Yu, W.-Y.; Dong, C.-L.; Velasco-Vélez, J.-J.; Chuang, C.-H.; Chen, L.-C.; Lee, J.-F.; Chen, J.-M.; Wu, H.-L. Controlling the Oxidation State of the Cu Electrode and Reaction Intermediates for Electrochemical CO_2 Reduction to Ethylene. *J. Am. Chem. Soc.* **2020**, *142*, 2857−2867.
(69) Wang, Y.; Xu, A.; Wang, Z.; Huang, L.; Li, J.; Li, F.; Wicks, J.; Luo, M.; Nam, D.-H.; Tan, C.-S.; Ding, Y.; Wu, J.; Lum, Y.; Dinh, C.-T.; Sinton, D.; Zheng, G.; Sargent, E. H. Enhanced Nitrate-to-Ammonia Activity on Copper−Nickel Alloys via Tuning of Intermediate Adsorption. *J. Am. Chem. Soc.* **2020**, *142*, 5702−5708.
(70) Wang, W.; Tse, E. C. M. Enhanced Nitrite Electrovalorization to Ammonia by a NiFe Layered Double Hydroxide. *Eur. J. Inorg. Chem.* **2022**, No. e202200291.
(71) Guo, D.-S.; Uzunova, V. D.; Su, X.; Liu, Y.; Nau, W. M. Operational calixarene-based fluorescent sensing systems for choline and acetylcholine and their application to enzymatic reactions. *Chem. Sci.* **2011**, *2*, 1722−1734.
(72) Barile, C. J.; Tse, E. C. M.; Li, Y.; Sobyra, T. B.; Zimmerman, S. C.; Hosseini, A.; Gewirth, A. A. Proton switch for modulating oxygen reduction by a copper electrocatalyst embedded in a hybrid bilayer membrane. *Nat. Mater.* **2014**, *13*, 619−623.
(73) Tse, E. C. M.; Hoang, T. T. H.; Varnell, J. A.; Gewirth, A. A. Observation of an Inverse Kinetic Isotope Effect in Oxygen Evolution Electrochemistry. *ACS Catal.* **2016**, *6*, 5706−5714.

https://doi.org/10.1021/jacs.4c18547
J. Am. Chem. Soc. 2025, 147, 14316−14325